View metadata, citation and similar papers at core.ac.uk

brought to you by CORE

provided by Elsevier - Publisher Connector

Journal of Solid State Chemistry 239 (2016) 204–213

Contents lists available at ScienceDirect

Journal of Solid State Chemistry

journal homepage: www.elsevier.com/locate/jssc

The many phases of CaC_2

Sumit Konar [a], Johanna Nylén [a], Gunnar Svensson [a], Diana Bernin [a], Mattias Edén [a], Uwe Ruschewitz [b], Ulrich Häussermann [a,*]

[a] Department of Materials and Environmental Chemistry, Stockholm University, SE-10691 Stockholm, Sweden
[b] Department of Chemistry, University of Cologne, Greinstrasse 6, 50939 Cologne, Germany

ARTICLE INFO

Article history:
Received 28 February 2016
Received in revised form
19 April 2016
Accepted 19 April 2016
Available online 21 April 2016

Keywords:
Acetylide carbides
Polymorphism
Structural stability

ABSTRACT

Polymorphic CaC_2 was prepared by reacting mixtures of CaH_2 and graphite with molar ratios between 1:1.8 and 1:2.2 at temperatures between 700 and 1400 °C under dynamic vacuum. These conditions provided a well controlled, homogeneous, chemical environment and afforded products with high purity. The products, which were characterized by powder X-ray diffraction, solid state NMR and Raman spectroscopy, represented mixtures of the three known polymorphs, tetragonal CaC_2-I and monoclinic CaC_2-II and -III. Their proportion is dependent on the nominal C/CaH_2 ratio of the reaction mixture and temperature. Reactions with excess carbon produced a mixture virtually free from CaC_2-I, whereas high temperatures (above 1100 °C) and C-deficiency favored the formation of CaC_2-I. From first principles calculations it is shown that CaC_2-I is dynamically unstable within the harmonic approximation. This indicates that existing CaC_2-I is structurally/dynamically disordered and may possibly even occur as slightly carbon-deficient phase $CaC_{2-\delta}$. It is proposed that monoclinic II is the ground state of CaC_2 and polymorph III is stable at temperatures above 200 °C. Tetragonal I represents a metastable, heterogeneous, phase of CaC_2. It is argued that a complete understanding of the occurrence of three room temperature modifications of CaC_2 will require a detailed characterization of compositional and structural heterogeneities within the high temperature form CaC_2-IV, which is stable above 450 °C. The effect of high pressure on the stability of the monoclinic forms of CaC_2 was studied in a diamond anvil cell using Raman spectroscopy. CaC_2-II and -III transform into tetragonal CaC_2-I at about 4 and 1GPa, respectively.

© 2016 The Authors. Published by Elsevier Inc. This is an open access article under the CC BY-NC-ND license (http://creativecommons.org/licenses/by-nc-nd/4.0/).

1. Introduction

Calcium carbide, CaC_2, is one of the most recognized inorganic compounds. In textbooks it is often introduced as the prototype for salt-like carbides. CaC_2 is a so-called acetylide, featuring C_2^{2-} dumbbell anions isoelectronic to dinitrogen [1–3]. The simple tetragonal CaC_2 type structure, in which dumbbells and Ca ions are arranged as in the NaCl structure, is very prominent and probably known to any chemistry student. A century ago CaC_2 represented a major commodity chemical, used in the production of acetylene and the fertilizer calcium cyanamide. Acetylene from coal derived CaC_2 remained a main source for industrial production of organic chemicals until the 1950s [4]. Today, CaC_2 is still an important commodity chemical, especially for China which has an annual production exceeding 20 million tons [5]. Its potential as reagent for current organic synthesis and nanotechnology has recently been reviewed by Rodygin et al. [6].

During the first half of the last century the structural and physicochemical properties of CaC_2 were intensively investigated, which revealed a stunningly complex polymorphism. Apart from a tetragonal form (CaC_2-I, with the famous CaC_2 type structure) [7] two monoclinic phases were identified (II and III) [8]. All three phases exist at room temperature. In addition, a high temperature form (IV) stable above 450 °C was established [9]. Significant efforts were undertaken to understand the thermodynamic relationships of the four crystal phases [7–9]. This included studies of the effects of oxygen, sulfur and nitrogen impurities in stabilizing the three low temperature forms [9]. The structural characterization of the monoclinic phases proved challenging [10] and remained inconclusive until around the year 2000 [11–13]. Today, the thermodynamic relations between the CaC_2 polymorphs are still uncertain. It is puzzling that the preparation of CaC_2 typically affords a mixture of room temperature phases [11,13]. The coexistence of several phases may be due to very small enthalpy differences between the polymorphs. Alternatively, one could suspect that, because of (small) compositional differences between the polymorphs, CaC_2 does not represent a single-component system.

* Corresponding author.
E-mail address: Ulrich.Haussermann@mmk.su.se (U. Häussermann).

http://dx.doi.org/10.1016/j.jssc.2016.04.030
0022-4596/© 2016 The Authors. Published by Elsevier Inc. This is an open access article under the CC BY-NC-ND license (http://creativecommons.org/licenses/by-nc-nd/4.0/).

From around the year 2010 CaC_2 has also become the focus for theoretical investigations, which uncovered further peculiarities. First, Kulkarni et al. explored the enthalpy landscape of CaC_2 by employing a simulated annealing algorithm and identified two more acetylide structures that energetically closely compete with the established polymorphs I, II, III [14]. Further, computational studies showed that with pressure, acetylide structures (with C_2 dumbbell units) become enthalpically unfavorable against polymorphs with novel polymeric carbon structures [15,16]. The experimental verification of the existence of such polycarbides is yet outstanding [17]. Most intriguing, however, is a recent report that questions the enthalpic stability of the composition CaC_2 in the ambient pressure Ca–C phase diagram [18]. From variable-composition evolutionary searches it was found that any CaC_2 polymorph should undergo phase segregation into a new carbide Ca_2C_3 and C. In light of this finding all room temperature forms of CaC_2 would be only metastable!

In this work we aim to shed some new light into the polymorphism of CaC_2. We show that tetragonal CaC_2-I (with the famous type structure) is actually dynamically unstable. We argue that its existence is only understandable when assuming CaC_2-I disordered and/or even slightly off-stoichiometric. We then report on the synthesis of CaC_2 from reactions employing CaH_2 and graphite mixtures, showing that the distribution of room temperature polymorphs depends on employed C/CaH_2 ratio, dwelling temperature and dwelling time. We propose that for a one-component system CaC_2 the tetragonal form I is metastable at all temperatures apart from a narrow interval prior transformation to the high temperature form CaC_2-IV.

2. Experimental section

2.1. Synthesis

All steps of sample preparations were carried out inside a glove box (Ar atmosphere, O_2 and H_2O level <0.1 ppm). Starting materials were elemental Ca (Aldrich, distilled, dendritic pieces, 99.99%, stored under Ar) and graphite powder (99.9995%, ABCR). First CaH_2 was produced by reacting Ca with pressurized H_2 gas (20 bar) in a stainless steel autoclave at 300 °C for 12 h. Graphite powder was degassed at 900 °C under dynamic vacuum for 6 h prior to use. For CaH_2–graphite reactions tantalum ampoules (L~50 mm, OD=10 mm) were employed as containers. Calcium hydride and graphite powder were thoroughly mixed with specific molar ratios (between 1:1.8 and 1:2.2) in an agate mortar and subsequently pressed into pellets (~200 mg of weight). Reactant pellets were sealed in Ta ampoules by welding. Ampoules were subsequently placed in fused silica jackets (L=400 mm, OD=26 mm).

For reactions at temperatures up to 1100 °C silica jackets were positioned in a vertical tube furnace and connected to a vacuum line. The empty space of the furnace was filled with silica insulation wool and a K-type thermocouple was introduced parallel to the silica jacket to monitor temperature close to the location of the metal ampoule. Ampoules were heated to a set temperature (between 700 and 1100 °C) at a rate of 10 °C/min and dwelled for 6 h and 24 h. During heating and dwelling ampoules were kept in a dynamic vacuum ($p<10^{-3}$ mbar), which was applied to promote the release and removal of H_2. Ta will become permeable to hydrogen at temperatures above 600 °C. Reactions at temperatures higher than 1100 °C were carried out in a RF furnace. Here, temperatures were monitored by a pyrometer.

At the end of the desired dwell time, ampoules were quenched to room temperature and opened in the glove box. Typically, the initial shape of the reactant pellet remained intact after reaction (see Supporting information, Fig. S1). The surface of the metal ampoule in contact with the pellet during the reaction was carefully inspected, but never found to be attacked. Recovered pellets were weighed (mg accuracy) and lightly ground for subsequent characterization and further experiments.

2.2. Scanning electron microscopy (SEM)

Powder samples were deposited on a holey carbon film on a Cu grid and transferred to the sample holder which was then placed in a closed container inside glove box. Sample was transferred to the microscope with air exposure less than 5 s SEM images were obtained using a JEOL JSM-7000F electron microscope at an acceleration voltage of 5 kV.

2.3. Powder X-ray diffraction

Powder X-ray diffraction (PXRD) patterns were collected on a Panalytical X'Pert alpha1 diffractometer (Cu $K\alpha_1$ radiation, $\lambda=1.540598$ Å) at room temperature. Moisture sensitive powder samples were mounted on a Si wafer zero background holder inside the glove box and covered with a Kapton foil. Diffraction patterns were measured in a 2θ range 20–90° with a step size of 0.013°. Rietveld analysis of PXRD data was performed using the program package FULLPROF [19]. Rietveld refinement proceeded according to the following strategy: (1) Fit of the background using linear interpolation between a set of background points; (2) Fit of the peak shape by Thompson-Cox-Hastings pseudo-Voigt convoluted with axial divergence asymmetry function for individual phases; (3) Spherical harmonics expansion of the crystallites shape function was employed for the major phase in a multi-phase refinement (size model=15 for monoclinic phases and size model=21 for the tetragonal phase) to reduce preferred orientation in a flat plate geometry; (4) To obtain a reliable phase fraction analysis, displacement parameters (B_{iso}) of like atoms in different phases were constrained to be the same.

2.4. NMR spectroscopy

Solid state ^{13}C NMR spectra were acquired at 9.4 T for two different CaC_2 specimens ("C1.8" and "C2.2") using a Bruker Avance-III spectrometer (–100.6 MHz ^{13}C Larmor frequency) equipped with a 7 mm double-resonance magic angle spinning (MAS) probehead. Finely ground powders were packed in 7 mm zirconia rotors inside a glove box (Ar atmosphere) and were spun at 7.0 kHz during the NMR experimentation. The ^{13}C NMR acquisitions involved single-pulse excitation with the radiofrequency (rf) pulses (60° flip angle) operating at a nutation frequency of 47 kHz. The data collection involved a 5 h equilibration delay, 45 min relaxation delay and a total of 56 (for C1.8) and 84 (for C2.2) accumulated signal transients. A Gaussian window function was applied prior to Fourier transformation of the recorded time-domain NMR signal. The absence of protons in polymorphic CaC_2 obtained from CaH_2–graphite reactions was verified by ^1H NMR experiments performed at 14.1 T and 24.0 kHz MAS on four samples obtained from different synthesis conditions, using a Bruker Avance-III spectrometer equipped with a 3.2 mm probehead. The ^{13}C and ^1H rf pulses were calibrated on a powder of adamantane. ^{13}C chemical shifts (in ppm) are quoted relative to neat tetramethylsilane (TMS).

2.5. Raman spectroscopy

Raman spectra were measured using a Labram HR 800 spectrometer. The instrument is equipped with an 800 mm focal length spectrograph and an air cooled (−70 °C), back thinned CCD

detector. Samples were excited using an air cooled double frequency Nd: YAG laser (532 nm) and an input laser power of 0.56 mW. Raman spectra were collected with an exposure time of 60 s, accumulation number of 10, and using a 1800 grooves/mm grating. *In situ* high pressure Raman spectroscopy experiments were performed at room temperature with a screw-driven Diamond Anvil Cell (DAC) DiaCell DXR-6 using a culet size of 300 μm. Powdered samples were packed into a 100–150 μm-sized hole drilled in a stainless steel gasket. No pressure transmitting medium was employed because of the interference from its luminescence and potential reactivity with the sample. CaC_2 was considered sufficiently soft to achieve satisfactory hydrostatic conditions, and care was taken to measure spectra from sample areas in proximity to the ruby chips, which were used as pressure indicators. Pressures were calculated from the fluorescence line shift according to Mao et al. [20]. The pressure was increased at steps of about 0.5 GPa and Raman spectra measured after a 15 min equilibration time.

2.6. Computations

Electronic structure calculations of polymorphs of CaC_2 were performed using the first principles all-electron projector augmented waves (PAW) method [21] as implemented in the Vienna Ab Initio Simulation Package (VASP) [22]. Exchange-correlation effects were treated within the generalized gradient approximation (GGA) using the Perdew-Burke-Ernzerhof (PBE) parameterization [23]. The structures were relaxed with respect to pressure, lattice parameters, and atomic positions. Forces were converged to better than 1×10^{-3} eV/Å. The energy cutoff was set to 675 eV. The integration over the Brillouin zone was done on a grid of special k-points of size $11 \times 11 \times 11$ determined according to the Monkhorst-Pack scheme [24] and the tetrahedron method with Blöchl correction [25]. Zone-centered phonon calculations were performed using VASP's density functional perturbation theory approach. Extended phonon calculations were carried out for CaC_2-I, -II, and -III using the Quantum Espresso package [26] using a $6 \times 6 \times 6$ k-point and $3 \times 3 \times 3$ q-point grid according to Monkhorst-Pack [24] and the PBE exchange-correlation parametrization [23]. The plane-wave cut off was set at 65 Ry. Ultrasoft pseudopotentials used were generated by the Vanderbilt method with $3s^2 3p^6 4s^2$ and $2s^2 2p^2$ as valence electrons for Ca and C, respectively [27].

3. Results and discussion

3.1. The enigma of CaC_2 phases

The polymorphism of CaC_2 has been known for a long time [7–9]. The existence at room temperature of three different crystal modifications of CaC_2 was established in 1937. In 1942 the discovery of a fourth modification, stable above 450 °C, was reported. Whereas the "famous" tetragonal structure of CaC_2-I was already determined in 1930 [28], the elucidation of the monoclinic forms II and III, either from twinned single crystal X-ray diffraction data or multi-phase PXRD patterns, proved difficult [10]. Around the year 2000 Meyer and co-workers [11,12] and Knapp et al. [13] finally reported on the conclusive structure characterization of CaC_2-II and –III.

Fig. 1 displays the structures of CaC_2-I, CaC_2-II, and CaC_2-III. Table 1 compares structure parameters and interatomic distances. For this comparison we use the structures obtained from computational relaxation ("DFT optimized" structures) which provides structural parameters on the same ground. Experimental structures, which are discussed later on, may be biased by the presence of disorder and/or compositional variations.

The structure of CaC_2-I (space group $I4/mmm$, Z=2) corresponds to a NaCl-type arrangement of Ca ions and C_2 acetylide dumbbells, which is tetragonally distorted due to the alignment of dumbbells along one axis (i.e., the tetragonal c axis). In the monoclinic structures the overall NaCl type, six-fold, coordination of dumbbells and Ca ions is maintained. However, tetragonally elongated Ca_6 octahedra (hosting dumbbells) are distorted and, additionally, with respect to their long axis, oriented in two directions. In CaC_2-II (space group $C2/c$, Z=4) dumbbells within the Ca_6 octahedra are exclusively aligned approximately along the long axis (Fig. 1b). In CaC_2-III (space group $C2/m$, Z=4) half of the dumbbells (those formed by the C2 atoms) are aligned toward opposite edges. When comparing interatomic distances, the monoclinic forms seem to provide a more efficient Ca–C coordination (that is, some Ca–C distances are shorter compared to tetragonal CaC_2-I). At the same time the mutual packing of Ca and dumbbells is slightly less effective. This is indicated in the molar volume, which is 1.3% and 1.5% larger for CaC_2-II and -III, respectively, compared to CaC_2-I. Lastly, the high temperature polymorph CaC_2-IV adopts a cubic NaCl type arrangement in which dumbbell units appear orientationally disordered [9a,13]. At 490 °C the molar volume of CaC_2-IV is by about 2% larger compared to CaC_2-I [13].

Typically the synthesis of CaC_2 yields a mixture of polymorphs. For example, technical CaC_2, which is prepared by reacting CaO or

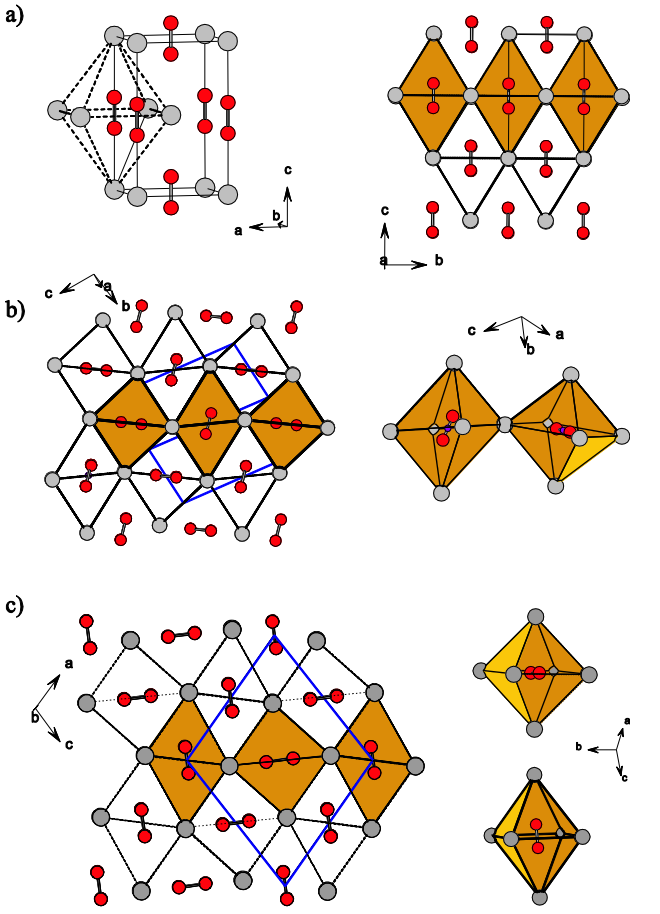

Fig. 1. Crystal structures of the ambient temperature polymorphs of CaC_2: (a) tetragonal CaC_2-I (space group $I4/mmm$, Z=2), (b) monoclinic CaC_2-II (space group $C2/c$, Z=4), (c) monoclinic CaC_2-III (space group $C2/m$, Z=4). The red and gray spheres correspond to C and Ca atoms, respectively. The octahedral environment of C_2 dumbbells by Ca atoms is emphasized. (For interpretation of the references to color in this figure legend, the reader is referred to the web version of this article.)

$CaCO_3$ with carbon at high temperatures (2200 °C and higher) in an electric arc furnace, represents a blend of tetragonal I and monoclinic II [13]. The high temperature reaction $CaO+3C=CaC_2+CO$ was extensively investigated by Franck et al. [7,8] and Bredig [9]. It was established that the proportion of polymorphs can be influenced by reaction conditions. "Excess of calcium" (or carbon deficient) reactions afforded pure samples of CaC_2-I. The formation of CaC_2-I is also promoted by the presence of impurities (being able to dissolve in CaC_2 as solid solutions, like CaS or $CaCN_2$ [7,8]). In the absence of S and N impurities (and employing stoichiometric reactions) CaC_2-I could be completely suppressed and pure samples of CaC_2-III were obtained [9]. With respect to impurities, it is important to mention that CaO does not influence the stability of any CaC_2 polymorph. It is practically insoluble in CaC_2 [29]. The influence of the C/Ca ratio on polymorph distribution was also observed for the formation reaction $Ca+2C=CaC_2$, using either sugar charcoal or graphite as carbon source [7,8]. Formation reactions can be performed at lower temperatures. The temperature interval 925–1250 °C typically affords a mixture of I and II. Franck et al. [7,8] and later Reckeweg et al. [11] showed that carbon deficiency and excess favor the formation of CaC_2-I and -II, respectively, whereas CaC_2-III was not obtained in this temperature interval. In contrast, Knapp et al. reported significant yields of CaC_2-III when carrying out formation reactions at 800 °C and employing conditions with excess C [13]. As a matter of fact, CaC_2-I, -II, and -III were obtained in almost equal proportions. With this we conclude our review of earlier CaC_2 synthesis experiments. An important point to consider – and not so done earlier – is that the synthesis of CaC_2 (at high temperatures) initially leads to the formation of the high temperature phase CaC_2-IV, from which the room temperature stable polymorphs I, II, III (or rather their mixtures) somehow evolve.

In view of the puzzling outcome of the CaC_2 synthesis experiments it appears difficult to establish thermodynamic relations between the polymorphs. However, Bredig already in 1942 provided a splendid analysis, assuming that CaC_2 is a one-component system [9a]. Later Glaser et al. [12] and Knapp et al. [13] confirmed parts of Bredig's analysis, and also added new features. We show the relations in Fig. 2. Interestingly, not only temperature but also mechanical deformation (grinding) can induce transitions between polymorphs. Bredig reported that pure CaC_2-III (obtained from high temperature arc furnace reactions $CaO+3C=CaC_2+CO$) transformed quantitatively into CaC_2-II when grinding at room temperature [9a]. Grinding CaC_2-III at elevated temperatures, however, yielded CaC_2-I. Later Glaser et al. confirmed the mechanically induced III to II transition [12].

Turning to temperature induced transitions, Bredig showed that CaC_2-II, obtained from grinding CaC_2-III, re-transforms to III upon heating [30]. Similarly, Glaser et al. obtained pure samples of CaC_2-III from temperature cycling mixtures of CaC_2-I/II to 520–540 °C [12]. Accordingly, there is no II-to-IV transition. Only CaC_2-I and -III transform to CaC_2-IV. From DSC measurements, Glaser et al. obtained distinct temperatures, 480 and 460 °C for the I-to-IV and the III-to-IV transition, respectively [12]. Transitions of CaC_2-I into either CaC_2-II or -III are uncertain although Knapp et al. observed a partial transformation of I into II in a low temperature [83 K (−190 °C)] PXRD experiment [13]. Today, Bredig's analysis [9] is still assumed valid and CaC_2-II is considered the low temperature ground state of CaC_2. CaC_2-I is regarded an ordered high temperature (HT) form, CaC_2-IV is a disordered HT form, and CaC_2-III is an ordered metastable form.

3.2. Energies of formation of CaC_2 phases

The evaluation of the structure stability of the ordered forms provides instructive insight into the polymorphism of CaC_2.

Table 1
Compilation of structure parameters from DFT calculations.

Phase	Structure parameter		Distance	
CaC_2-I *I4/mmm*	a (Å)	3.8846	Ca–C	2.569 × 2 2.818 × 8
	c (Å)	6.3990		
	V/Z (Å^3)	48.28	CC–Ca[a]	2.747 × 4 3.200 × 2
	C 4e (0 0 z)	0.4014		
			C–C	1.262
CaC_2-II *C2/c*	a (Å)	6.6158	Ca–C	2.574 × 2 2.638 × 2 2.790 × 2 2.825 × 2 3.191 × 2
	b (Å)	4.1513		
	c (Å)	7.4669		
	β (°)	107.5		
	V/Z (Å^3)	48.90		
	Ca 4e (0 x ¼)	0.1757	CC–Ca[a]	2.736 × 2 2.859 × 2 3.170 × 2
	C 8f (x y z)	0.2211 0.1421 -0.0618		
			C–C	1.260
CaC_2-III *C2/m*	a (Å)	7.1548	Ca–C1	2.567 2.718 × 2 2.947 × 2
	b (Å)	3.8367		
	c (Å)	7.4569		
	β (°)	106.9	Ca–C2	2.607 × 2 2.762 2.777
	V/Z (Å^3)	49.0		
	Ca 4i (x 0 z)	0.2036 0.2471		
	C1 4i (x 0 z)	0.4532 0.0598		
	C2 4i (x 0 z)	0.0793 0.5648	CC1–Ca[a]	2.697 × 4 3.068 × 2
			CC2–Ca[a]	2.764 × 4 3.187 × 2
			C1–C1	1.261
			C2–C2	1.259

[a] "CC" refers to the center of a C_2 dumbbell.

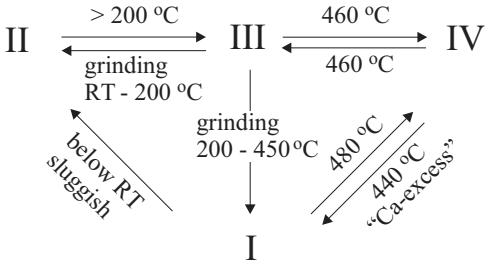

Fig. 2. Scheme of phase relations among CaC_2 polymorphs, according to Refs. [9,12,13]. Note, the high temperature form IV transforms to either III or I upon cooling. CaC_2-III upon grinding turns to II or I depending on temperature of grinding.

Recently, Kulkarni et al. performed an extensive search for structure candidates for CaC_2 and identified in addition to known CaC_2-I, II, III, (IV) an orthorhombic (CaC_2-V) and a further monoclinic structure (CaC_2-VI) as viable ambient pressure alternatives [14]. CaC_2-V and -VI can be derived from tetragonal CaC_2-I by a simple rotational distortion of the C_2 dumbbells. Fig. 3 depicts the energies of formation $\Delta E(CaC_2)=E(CaC_2)-E(\text{fcc-Ca})-E(\text{graphite})$ (referring to the formation reaction $Ca+2C(\text{graphite})=CaC_2$) for the various polymorphs based on our DFT calculations. We also include the recently proposed polycarbide *Cmcm*-CaC_2 which is the enthalpically most stable CaC_2 polymorph at pressures 1–12 GPa [15].

All polymorphs have negative energies of formation, that is, they represent thermodynamically stable compounds with respect to the constituting elements (note that this is not the case for MgC_2 [31]). It is remarkable that the enthalpies of the six phases differ by no more than 25 meV/formula unit (about 2.4 kJ/mol).

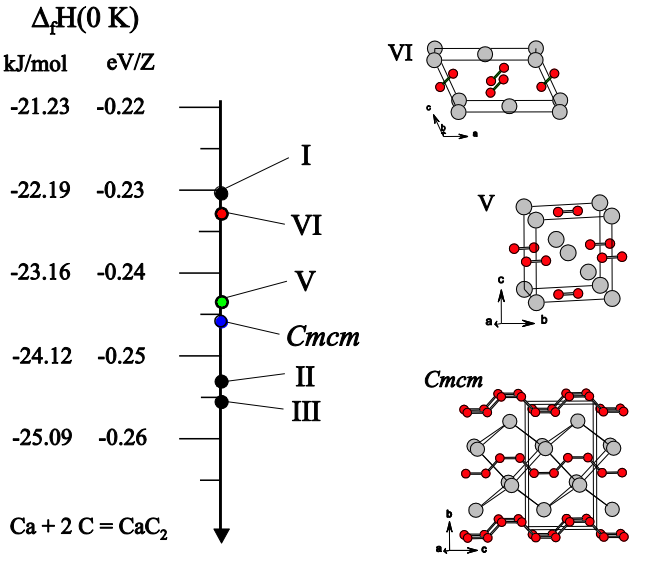

Fig. 3. Compilation of the formation energies $\Delta E(CaC_2)=E(CaC_2)-E(fcc\text{-}Ca)-E$ (graphite) for various CaC_2 polymorphs based on DFT calculations.

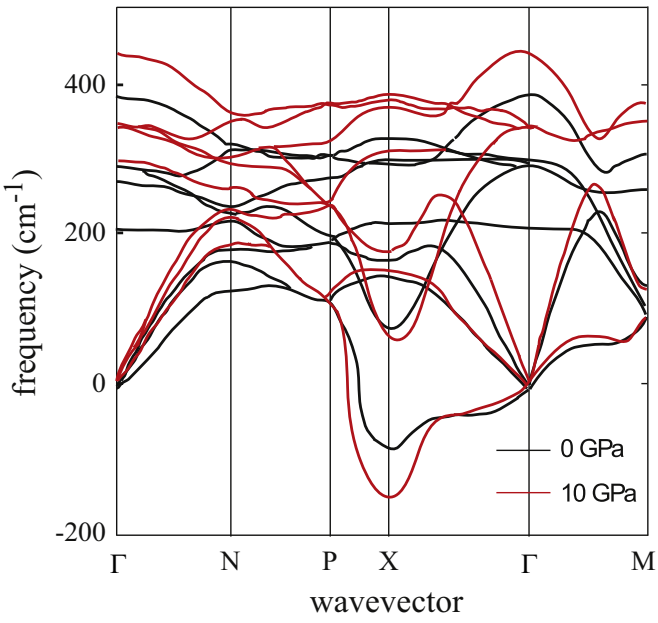

Fig. 4. Calculated phonon dispersion relations of CaC_2-I at ambient pressure (black line) and at 10 GPa (red line). (For interpretation of the references to color in this figure legend, the reader is referred to the web version of this article).

And one can easily envision that more phases with (hypothetical) structures varying in the orientation of C_2 dumbbells may fall in this energy window. According to these calculations, the ground state corresponds to CaC_2-III which is essentially degenerate with CaC_2-II. Although enthalpy differences are small, it is surprising that tetragonal CaC_2-I comes out as the least stable in this selection.

We therefore investigated the dynamic stability of CaC_2-I by calculating phonon dispersion relations (within the harmonic approximation). The criterion for a dynamically stable structure is real eigenvalues (phonon energies/frequencies) for all k(q) points in the Brillouin zone. This is the case for the monoclinic forms CaC_2-II and -III. However, for tetragonal CaC_2-I it is surprisingly not. Fig. 4 shows the phonon dispersion relations for CaC_2-I, where imaginary frequencies are represented as negative numbers. In particular, the transverse acoustic phonon branch is instable for the complete symmetry line D (Γ–X) [which expresses the [110] polarization] and large parts of the line W (X–P). The imaginary zone boundary X implies that CaC_2-I is also elastically instable and one may deduce a monoclinic distortion.

This result is unexpected: the famous tetragonal CaC_2 structure type is not stable for CaC_2! Importantly, the dynamic instability becomes more pronounced with pressure (cf. Fig. 4, red curve, 10 GPa). There may be several reasons why the harmonic approximation gives instable phonons. One possibility is that imaginary phonon modes will be anharmonically stabilized at high temperatures. The dynamic stabilization of structures with temperature has been demonstrated for transition metals, e.g. the fcc structures of Mo and W [32]. This would imply that CaC_2-I is only stable at high temperatures and with pronounced anharmonic dynamics. Another possibility is that the actual structure of CaC_2-I deviates from the ideal model by e.g. the presence of structural disorder, defects, or even non-stoichiometry.

3.3. *Synthesis and characterization of CaC_2 from CaH_2 and graphite*

In light of the disparate results of previous CaC_2 synthesis experiments we decided to investigate reactions between calcium hydride and graphite, according to $CaH_2+2C=CaC_2+H_2$. Our intention was to perform carbide synthesis in a well controlled chemical environment, which at the same time allows for low synthesis temperatures, and to compare against previous results from CaO+C and Ca+C reactions. Employing CaH_2 as Ca source has the advantage that both reactants represent powders that can be intimately mixed and pressed to homogenous pellets, thus allowing for stoichiometric control of C/Ca ratios. At temperatures around 700 °C CaH_2 will decompose cleanly to Ca with a high surface area which greatly benefits kinetics. Alkali and alkaline earth metal hydrides have been used previously as precursors for the preparation of (Zintl phase) silicides and germanides [33], and also Li_2C_2 [34], which afforded products at lower temperatures and with higher purity.

We considered the graphite/CaH_2 molar ratios 1.8:1, 2:1, and 2.2:1 (slight excess of Ca, stoichiometric, and slight excess of C). The temperature interval investigated was 700–1100 °C. Employed dwelling times were 6 and 24 h. Additionally, reactions with short dwelling periods (15 min) were carried out at 1400 °C. After dwelling, reactions were quenched to room temperature and the products analyzed. The excess of Ca and C in the mixtures 1.8:1 and 2.2:1, respectively, was not recognizable in PXRD patterns (see Supporting information, Fig. S2). A dynamic vacuum was applied to promote the release and removal of H_2. No mass losses exceeding those expected from H_2 release occurred.

So obtained CaC_2 was virtually free from impurities. Notably, ^1H MAS NMR revealed no resonances beyond those associated with background signals from an empty rotor. If present in trace amounts, the proton content of CaC_2 obtained from CaH_2–graphite reactions is below 100 wt ppm. The samples represented a mixture of polymorphs. The proportions are clearly dependent on the C/CaH_2 ratio, but also dwelling temperature and time. From the color of the product, the major phase could be assessed: CaC_2-I black, CaC_2-II white, CaC_2-III gray. Fig. 5 shows representative Rietveld plots and the colors of products obtained from 1400 °C reactions (a complete compilation is given as supporting information, Fig. S3). Fig. 6 summarizes the phase fraction of CaC_2 polymorphs in the products of the various reactions, as determined by Rietveld refinement (for details, see Supporting information Table S1). Three scenarios can be distinguished: (i) Products from stoichiometric and C excess reactions were almost free from CaC_2-I when employing high temperatures (1100 °C and 1400 °C) and also with the condition 900 °C/24 h. The ratios of II/III were very similar, perhaps there is a tendency that

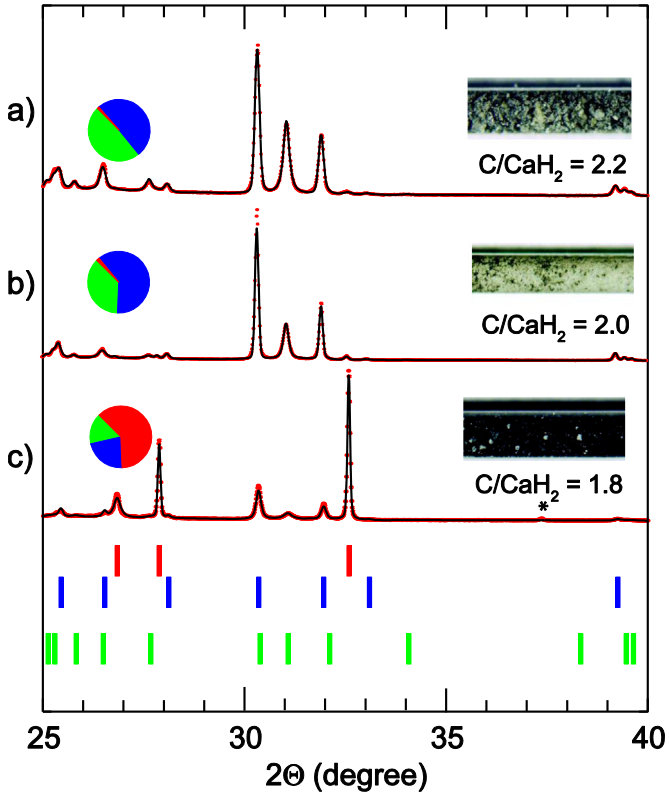

Fig. 5. Multiphase Rietveld fits to powder X-ray diffraction patterns (Cu $K\alpha_1$ radiation) of products obtained from reactions at 1400 °C using three starting material compositions (C/CaH_2=2.2 (a), 2.0 (b) and 1.8 (c)) and a dwelling time of 0.25 h. The location of Bragg peaks are marked by vertical bars. The asterisk in (c) marks a reflection from CaO impurity. CaC_2-I red, CaC_2-II blue, CaC_2-III green; this color code is maintained in the following figures. (For interpretation of the references to color in this figure legend, the reader is referred to the web version of this article.)

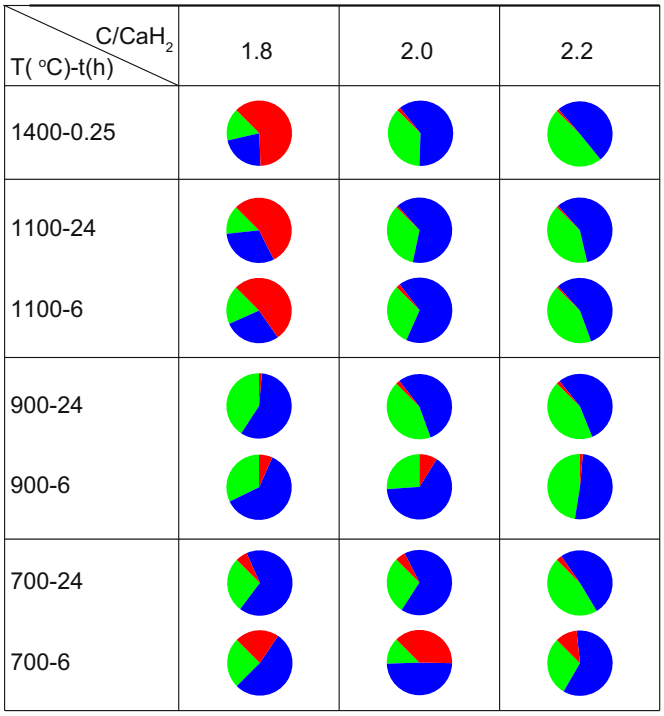

Fig. 6. Summary of synthesis results. The relative phase fractions of CaC_2 polymorphs are presented as pie charts, with different colors corresponding to different phases (CaC_2-I red, CaC_2-II blue, CaC_2-III green). For absolute phase fractions (wt%) and details, see the Supporting information. (For interpretation of the references to color in this figure legend, the reader is referred to the web version of this article.)

excess C slightly favors the formation of CaC_2-III. (ii) The formation of CaC_2-I was clearly favored in C deficient reactions at high temperatures (1100 °C and 1400 °C). However, CaC_2-I was essentially suppressed in the C deficient reaction 900 °C/24 h. Generally, 900 °C/24 h reactions did not yield significant amounts of CaC_2-I, instead, there is an increase of the fraction of CaC_2-III when going from C deficient to C excess. (iii) At lower temperatures (700 °C and 900 °C) the polymorph distribution depends on the dwelling time. This indicates that at these temperatures initially formed CaC_2-IV (which is the stable polymorph at temperatures above 450 °C) is "heterogeneous" and "homogenizes" (or equilibrates) over time (cf. dwellings for 6 h and 24 h). It also indicates that heterogeneous CaC_2-IV favors the formation of CaC_2-I.

Our synthesis reactions employing CaH_2 confirm unambiguously the influence of the C/Ca ratio on the proportion of polymorphs in the product, as described earlier by Bredig [9] and Reckeweg et al. [11]. Further, our reactions allow the synthesis of CaC_2 at exceptionally low temperatures (700 °C) which in turn revealed a dwelling time dependency of the polymorph distribution.

We now turn to the analysis of the crystal structures of CaC_2-I, -II, and -III. The results from our refinements are compiled in Tables 2 and 3, and compared with the structures previously reported by Meyer and co-workers [11,12] and Knapp et al. [13]. (For details, see supporting information). The literature structures differ somewhat for CaC_2-II and CaC_2-III, and our results seem to be more similar to Meyer and co-workers. We note that refinement results are slightly different across the products from the various reactions (see Supporting information, Table S2) indicating problems in obtaining precise structural parameters from Rietveld refinements of multiphase samples. When comparing Tables 2 and 3 with Table 1 it is apparent that the experimental structures of CaC_2-II and -III deviate significantly from the DFT optimized ones (whereas the simple CaC_2-I structure agrees well). We believe that these discrepancies are due to shortcomings in the Rietveld refinements, possibly in conjunction with structural disorder. It is worth mentioning that in the experimental structures the C–C distance of dumbbell units ranges from 1.18 to 1.33 Å, whereas DFT calculations yield strictly 1.26 Å, independent of the polymorph.

Fig. 7 shows representative SEM micrographs of particles from a CaC_2-II/III phase mixture and from a mixture dominated by CaC_2-I. Crystallites are built from lamellae with about 0.1 μm thickness, which are finely interwoven. For CaC_2-I crystallites the lamellar microstructure is peculiarly curved. The overall texture is most likely influenced by the microstructure of CaC_2-IV from which the room temperature phases evolve. We remind on the multitude of structures with very similar energies that arise from various dumbbell orientations (cf. Fig. 3) and one can envision broad possibilities for structural disorder in the room temperature phases. This includes (i) disorder from random alignment of dumbbells within Ca_6 octahedra and (ii) vibrational (dynamic) disorder. But also (iii) C_2 defects and/or replacements $2\,C_2^{2-} \leftrightarrow C^{4-}$may be considered, which would result in compositional variations. Traditional Rietveld refinement of CaC_2 polymorphs (as also applied in this work) will not capture the decisive structural features which relate to such disorder. There are several clear indications for disorder described in the literature, especially for CaC_2-I. These include anomalous peak broadening of *h0l* and *hkl* reflections in PXRD patterns [13,35] and a pronounced broadening of signals in ^{13}C MAS-NMR spectra [11,12,36].

Fig. 8 displays the ^{13}C MAS NMR spectra recorded from specimens with C/CaH_2 ratio of 1.8 and 2.2 that were quenched from

Table 2
Compilation of experimental structure parameters.

Phase	Structure parameter	Synchrotron PXRD at 83 K (Ref. [13])	I (SC-XRD, RT) (Ref. [11])II, III (PXRD, RT) (Ref. [11], [12])	I (1400C-0.25h-1.8) II (900C-6h-2) III (900C-24h-2.2) This work (PXRD, RT)
CaC_2-I	a (Å)	3.8658(1)	3.8863(4)	3.8845(1)
I4/mmm	c (Å)	6.4007(2)	6.3862(9)	6.3969(2)
	V/Z (Å^3)	47.83	48.2	48.26
	Ca 2a (0 0 0)			
	C 4e (0 0 z)	0.407(1)	0.406(2)	0.408(1)
CaC_2-II	a (Å)	6.5995(2)	6.632(1)	6.6479(1)
C2/c	b (Å)	4.1899(2)	4.1889(7)	4.2007(3)
	c (Å)	7.3109(3)	7.311(1)	7.3335(5)
	β (°)	107.034(2)	107.24(1)	107.259(3)
	V/Z (Å^3)	48.32	48.5	48.89
	Ca 4e	0		0
	(0 x ¼)	0.1821(5)		0.185(1)
		0.25		0.25
	C 8f	0.282(1)		0.276(3)
	(x y z)	0.146(1)		0.135(3)
		0.0562(8)		0.051(3)
CaC_2-III	a (Å)	7.2076(3)	7.226(1)	7.2317(4)
C2/m	b (Å)	3.8283(2)	3.8526(7)	3.8540(1)
	c (Å)	7.3677(4)	7.376(1)	7.3780(3)
	β (°)	107.19	107.345(1)	107.366(2)
	V/Z (Å^3)	48.55	49.0	49.1
	Ca 4i	0.1969(7)	0.2055(2)	0.206(1)
	(x 0 z)	0	0	0
		0.2544(7)	0.2464(3)	0.248(2)
	C1 4i	0.421(2)	0.4506(9)	0.444(4)
	(x 0 z)	0	0	0
		0.021(3)	0.061(1)	0.052(4)
	C2 4i	0.048(3)	0.0799(8)	0.075(4)
	(x 0 z)	0	0	0
		0.58(2)	0.562(1)	0.563(4)

Table 3
Compilation of experimental interatomic distances (in Å).

Phase	Distance	Synchrotron PXRD at 83 K (Ref. [13])	I (SC-XRD, RT) (Ref. [11]) III (PXRD, RT) (Ref. [12])	I (1400C-0.25h-1.8) II (900C-6h-2) III (900C-24h-2.2) This work (PXRD, RT)
CaC_2-I	Ca–C	2.605(6)	2.60(1)	2.610(6)
		2.798(1)	2.812(2)	2.809(1)
	CC–Ca[a]	2.7335(1)	2.7480(2)	2.7468(1)
		3.2004(1)	3.1931(4)	3.1985(1)
	C–C	1.190(9)	1.20(1)	1.177(9)
CaC_2-II	Ca–C	2.581(5)		2.58(2)
		2.653(7)		2.67(2)
		2.815(5)		2.76(2)
		2.816(5)		2.90(1)
		3.080(7)		3.10(2)
	CC–Ca[a]	2.752(1)		2.767(3)
		2.8125(2)		2.8295(4)
		3.156(2)		3.154(3)
	C-C	1.187(7)		1.21(2)
CaC_2-III	Ca–C1	2.68(2)	2.540(8)	2.56(3)
		2.74(1)	2.733(4)	2.79(2)
		2.92(1)	2.932(5)	2.89(2)
	Ca–C2	2.68(1)	2.609(4)	2.62(2)
		2.42(2)	2.739(8)	2.76(3)
		2.90(2)	2.826(8)	2.79(3)
	CC1–Ca[a]	2.609(6)	2.713(2)	2.707(8)
		3.062(3)	3.060(1)	3.055(5)
	CC2–Ca[a]	2.760(3)	2.759(1)	2.766(4)
		3.272(6)	3.184(2)	3.192(8)
	C1–C1	1.27(3)	1.30(1)	1.27(5)
	C2–C2	1.18(2)	1.241(8)	1.20(3)

[a] "CC" refers to the center of a C_2 dumbbell.

1400 °C; they are in the following referred to "C1.8" and "C2.2", respectively. Besides a broad signal centered around 110 ppm that stems from a minor impurity of graphite, the NMR spectra display resonances from the C_2^{2-}environments in three distinct CaC_2 polymorphs (I, II and III). Owing to the sizable ^{13}C chemical shift anisotropy [12], the resonance associated with each crystallographically unique $^{13}C_2^{2-}$ pair is distributed over a set of spinning sidebands that results at the modest MAS rate (7.0 kHz) utilized herein. The isotropic chemical shifts at each centerband position ~200 ppm in the NMR spectra are shown in Fig. 8(a) and (b), whereas Fig. 8(c) assigns each resonance to its corresponding CaC_2 polymorph (I, II, and III).

According to the PXRD analysis, the C1.8 and C2.2 specimens comprises polymorph ratios I: II: III of 62:22:16 and 1:51:48, respectively (cf. Fig. 6). The NMR spectrum from C2.2 reveals all expected resonances, with that ~200 ppm assigned to CaC_2-II, while the peaks at isotropic chemical shifts of ~203 ppm and ~197 ppm are attributed to the two crystallographically distinct C_2 dumbbells in CaC_2-III. Compared to Glaser et al. [12] we observe a slightly higher chemical shift (by 2 ppm) for CaC_2-II whereas those for CaC_2-III accord very well (203 ppm and 197 ppm). The NMR signal with an isotropic chemical shift ~206 ppm is attributed to CaC_2-I. This shift value is in excellent agreement with that reported by Wrackmeyer et al. for "technical grade" CaC_2 [36] but is significantly higher than those (196–199 ppm) reported by Meyer and co-workers [11,12].

Besides the different signal intensities stemming from variable contributions of each CaC_2 polymorph to the specimens, the primary distinction between the two ^{13}C NMR spectra is the overall broader resonances observed from the C1.8 sample relative to those in the C2.2 counterpart; this is evident by comparing the two NMR responses from the CaC_2-II component in Fig. 8(c). We attribute the resonance broadening to distributions of isotropic chemical shifts stemming from different extents of structural disorder in the two samples. In this respect especially the CaC_2-I phase appears to be heterogeneous. The reported chemical shift dispersion from 196 to 206 ppm points to significant structural

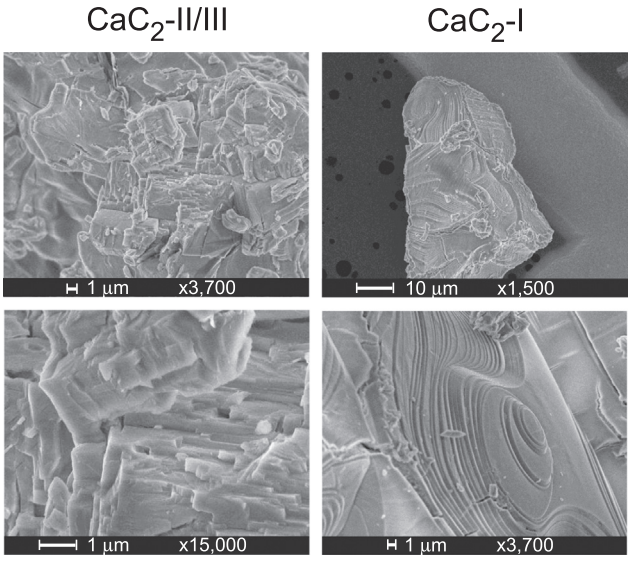

Fig. 7. Scanning electron micrographs of CaC_2 specimens obtained from reactions at 1100 °C and using a dwelling time of 24 h: right hand panel - predominantly tetragonal form CaC_2-I (mixture C/CaH_2=1.8), left hand panel - monoclinic forms CaC_2-II and –III (mixture C/CaH_2=2.2).

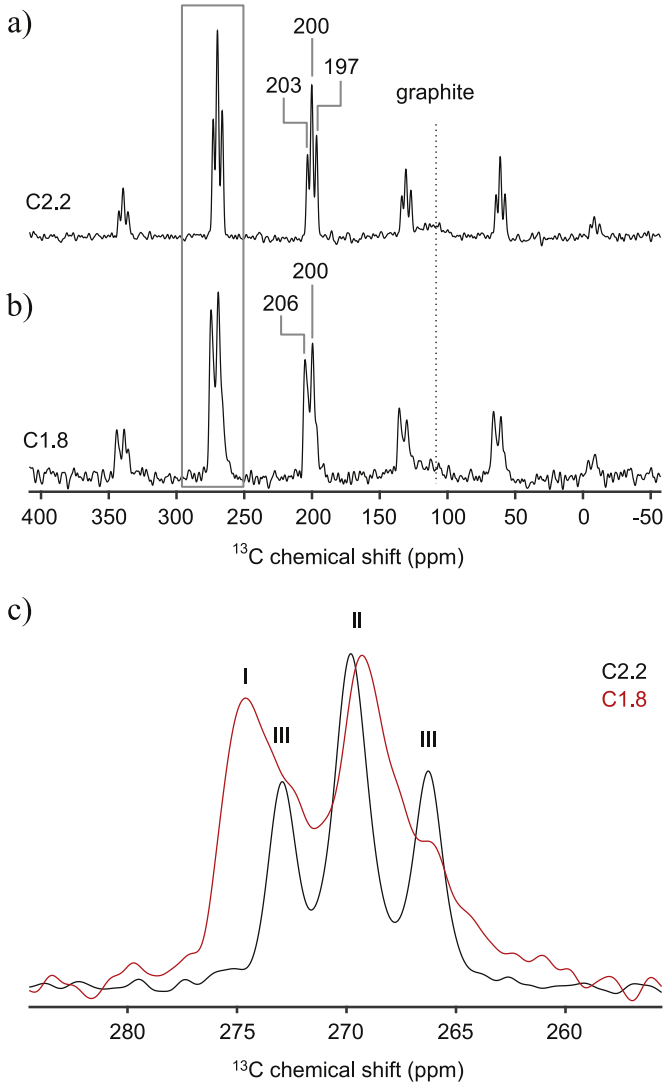

Fig. 8. ^{13}C MAS NMR spectra recorded from $C/CaH_2=2.2$ (sample C2.2, (a)) and $C/CaH_2=1.8$ (sample C1.8, (b)) reactions quenched from 1400 °C. Each number marks the corresponding peak maximum. (c) Zoom around the first order sideband region indicated by the rectangle in (a, b), showing the assignment of each ^{13}C resonance to its corresponding CaC_2 polymorph in C2.2 (black trace) and C1.8 (red trace). (For interpretation of the references to color in this figure legend, the reader is referred to the web version of this article.)

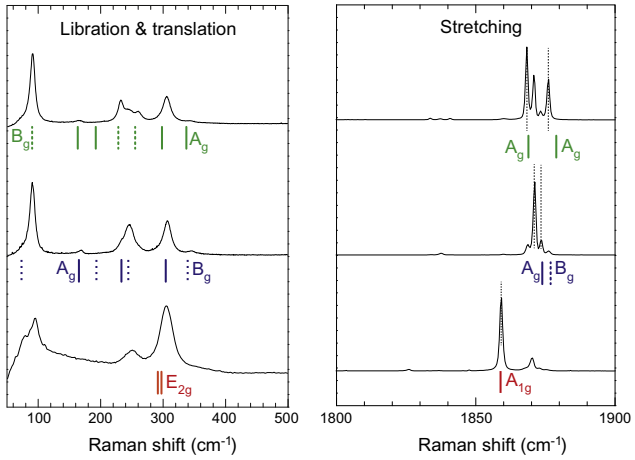

Fig. 9. Raman spectra of CaC_2 polymorphs from multi-phase products obtained from reactions at 1100 °C and for a dwelling time of 24 h (cf. Fig. 6). The upper spectrum corresponds to a mixture of II and III. The middle spectrum is mainly form II (with a very minor III contribution). The lower one is mainly form I (with a minor II contribution). Calculated Raman frequencies are marked by vertical bars (I=red, II=blue, III=green; A_g, A_{1g}=single bar, E_{2g}=double bar, B_g=dashed bar). The week signals in the region 1825–1840 cm^{-1} (right panel) are contribution from ^{13}C and ^{12}C to the C–C stretch vibration. (For interpretation of the references to color in this figure legend, the reader is referred to the web version of this article.)

Table 4
Compilation of Raman active modes (in cm^{-1}) for CaC_2-I, CaC_2-II, and CaC_2-III. (lib=libration mode, trans=translation mode).

CaC_2-I (D_{4h})		CaC_2-II (C_{2h})		CaC_2-III (C_{2h})	
Exp.	Calc.	Exp.	Calc.	Exp.	Calc.
1859	1859 A_{1g}	1874	1877 B_g	1876	1879 A_g
		1871	1874 A_g	1869	1869 A_g
305	297 E_g (lib)	346	339 B_g (lib)		337 A_g (lib)
		306	304 A_g (lib)		298 A_g (lib)
		244	244 B_g (lib)	260	255 B_g (lib)
			233 A_g (lib)	232	228 B_g (lib)
			193 B_g (trans)		192 A_g (trans)
		169	165 A_g (trans)	165	163 A_g (trans)
		79	73 B_g (trans)	90	90 B_g (trans)

and/or even compositional variations. In addition, as already described by Reckeweg et al. [11], there is a pronounced dependence of ^{13}C NMR peak-width of CaC_2-I on applied synthesis conditions.

Next we discuss the results of the Raman spectroscopy analysis, probing sample areas of 1–2 μm. The Raman spectra of I, II, III are shown in Fig. 9. Additionally, the wavenumbers of Raman active modes are compiled in Table 4 and compared with the ones obtained from DFT calculations. The spectra can be divided into two regions: C–C stretches occur at wavenumbers between 1850 and 1900 cm^{-1}, whereas libration modes of C_2 dumbbells and translation modes, which constitute largely of displacements of the Ca ions, occur at wavenumbers below 400 cm^{-1}. Just two bands constitute the Raman spectrum of tetragonal CaC_2-I: the stretching mode at 1858 cm^{-1} and the double degenerate libration at 305 cm^{-1}. These wavenumbers agree well with the DFT calculated ones (at 1859 and 297 cm^{-1}). And there is also good agreement between experimental bands and calculated wavenumbers for CaC_2-II and -III. Note that for CaC_2-II and -III the primitive unit cell contains two formula units. The interaction (vibrational coupling) between two dumbbell units in the crystal (correlation splitting) is clearly resolved in our spectra.

The C–C stretches of CaC_2-II and -III are at significantly higher wavenumbers compared to CaC_2-I. The larger unit cell and lower symmetry of the monoclinic forms implies a larger number of libration and translation modes. The associated bands in the spectrum are broad and overlapping. The excellent agreement of DFT calculated C–C stretching modes with experimentally observed bands strongly supports the validity of the DFT optimized structures and, thus, the presence of uniform C_2 dumbbell units (with a C–C distance near 1.26 Å) in all three polymorphs. The disorder established from NMR on CaC_2 bulk samples is, thus, difficult to reconcile on the μm scale. The observation of narrow stretching bands and correlation splitting implies crystalline order within the probed domains. However, the broad libration/translation bands (in contrast with sharp stretching ones) indicate significant anharmonic behavior.

3.4. *Pressure stability of CaC_2 phases*

Before returning to the influence of T to phase relations we also address the pressure stability of CaC_2 polymorphs. In recent years this topic has attracted considerable attention because of a

potential pressure induced transformation of the acetylide carbide into a polycarbide [15,16]. Previously it has been reported that tetragonal CaC_2-I can be pressurized up to about 18 GPa with only minor structural changes. At higher pressures an irreversible amorphization takes place [17,37]. This extended pressure stability contrasts the results from the phonon calculations which revealed an increasing dynamic instability of CaC_2-I with pressure (cf. Fig. 4). The existence of CaC_2-I at high pressures is especially difficult to reconcile without assuming structural/compositional disorder. The high pressure behavior of the monoclinic forms CaC_2-II and -III is not clear. To study their pressure stability Raman spectra of samples free from CaC_2-I were recorded in a DAC.

Fig. 10a shows Raman spectra of a II/III mixture with increasing pressure (restricted to the spectral region of C–C stretches). It is clearly noticeable that with pressure both monoclinic modifications transform independently into CaC_2-I. The transformation of CaC_2-III is seen already at very low pressures (below 0.9 GPa). At 3.6 GPa CaC_2-III disappeared and only II and I coexist. At 5.5 GPa also CaC_2-II has completely transformed into I. The onset of the II-to-I transition is presumably at lower pressures. Note that with pressure bands of C–C stretches broaden considerably. A rather interesting observation was made upon decompression (Fig. 10b): At around 2 GPa C–C stretching bands of monoclinic CaC_2-II became visible again which indicates the reversibility of the pressure induced II-to-I transition. The pressure induced transformation of III and II into I is expected when considering molar volumes (cf. Table 1). Importantly, the II-to-I transformation and its partial reversal upon pressure release shows unambiguously that there is a direct phase relation between I and II, with the latter being the more stable form at ambient conditions.

3.5. Relation of CaC_2 phases

So, what are the thermodynamic relations between CaC_2 phases? Bredig in 1942 developed an apparently reasonable view – based on the assumption that CaC_2 is a one-component system – where II represents the ground state, I a medium temperature phase, IV the HT phase, and III is metastable at all temperatures [9]. This view was questioned by Meyer and co-workers [11,12] who seem to prefer III as stable medium temperature phase in a sequence II – III – IV and posed the question how I should be related to this sequence. First of all, it is not clear whether CaC_2 actually represents a single-component system because of possible (small) compositional differences between the polymorphs. Especially, the preferred formation of CaC_2-I from Ca excess reaction mixtures may suggest that this phase possesses a homogeneity range allowing for slight C deficiency. If nonetheless assuming a one-component system we suggest an altered view to the one by Bredig.

Fig. 11 depicts a schematic representation of our suggested phase relations. Compared to Bredig's view, I and III are interchanged. That is, the sequence of stable phases with increasing T is II –(~200 °C)– III –(~460 °C)– IV as suggested by Meyer. I is assumed to be generally metastable, but is presented as a band (with variable free energy (F) width) in the plot. The band representation accounts for various dynamical and structural scenarios as well as compositional heterogeneities that may be realized within phase I. This includes also effects induced by stress and microstrain. The boundary of the band toward low F is uncertain. For pure samples of CaC_2 the F variability of I is assumed narrow, in line with the width of the band drawn in Fig. 11, allowing a small window of thermodynamic stability at high temperatures slightly below the transformation to IV. The presence of impurities, such as S^{2-} and CN_2^{2-}, can stabilize I tremendously (as indicated by a dotted line), making it more stable than III [7–9].

For reasons unknown, metastable I has a distinct kinetic stability. Upon heating from room temperature the only transition of I is into IV. Depending on its form (i.e. location within the F band), the transition temperature varies (between 450 and 480 °C). Most important is the role of CaC_2-IV for understanding the phase relations of CaC_2. IV exists over a very wide T range; CaC_2 melting is estimated at around 2200 °C [7,8]. We propose that CaC_2-IV has to be considered as "heterogeneous". That is IV actually comprises several phases because of various states of disorder in addition to a possible small homogeneity range. At high temperatures (close to the melting point) dumbbells will be dynamically disordered, possibly freely rotating in the average NaCl structure. Upon lowering temperature different states of static or mixed static/dynamic disorder could freeze out, opening for complex non-

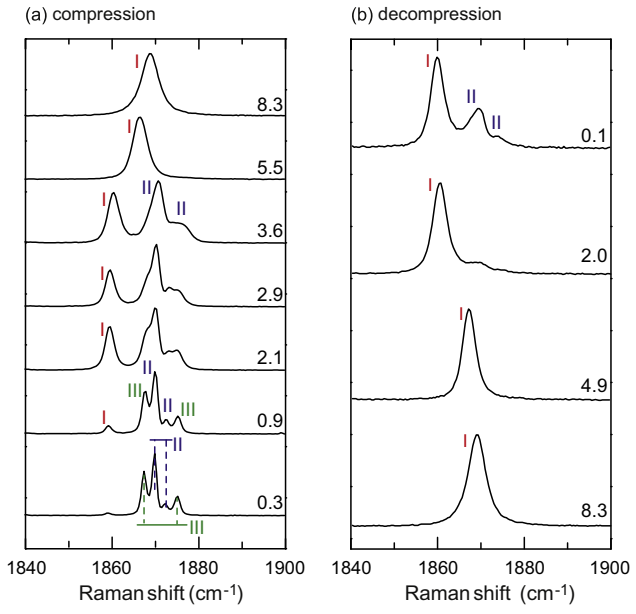

Fig. 10. Raman spectra of a mixture of CaC_2-II and –III upon compression (a) and decompression (b). Inset numbers denotes pressure in GPa.

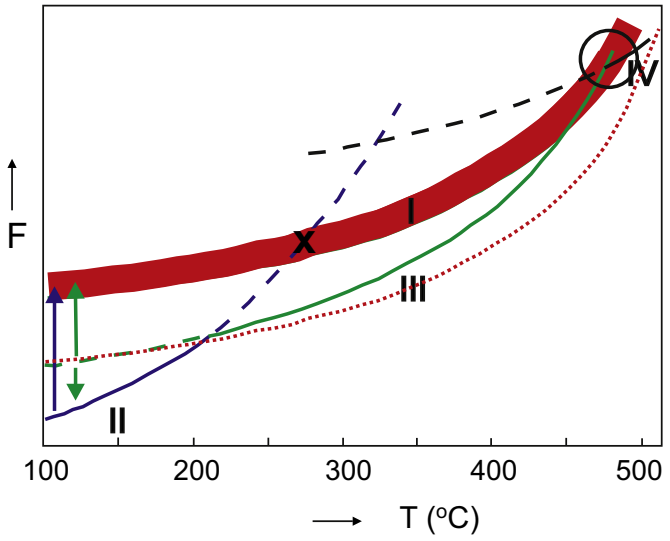

Fig. 11. Sketch of the CaC_2 phase relations (modified from Bredig [9a]) assuming a one-component system, but with a heterogeneous phase I. (I=red, II=blue, III=green, IV=black). The existence of different forms of I is indicated by the red band. The lower boundary (highest possible stability) is indicated by a red dotted line. The circle marks the position of IV-to-I and IV-to-III transitions, the cross marks the position of the I-to-II transition. The blue arrow indicates the pressure induced II-to-I transition. The green arrows indicate the pressure induced III-to-I and mechanically induced III-to-II transitions. (For interpretation of the references to color in this figure legend, the reader is referred to the web version of this article.)

equilibrium scenarios. Depending on synthesis conditions (C/Ca ratio, dwelling temperature and time, annealing rate) the transition into the low temperature form of CaC_2 may occur from a different state of IV, preferring either the metastable I or stable III pathway (black circle in Fig. 11). III is known to be kinetically stable with respect to transformation into II upon cooling. Consequently, II has to form from I upon cooling (i.e. the location of the cross in Fig. 11 at about ~250 °C). If true, then temperature cycling I between 200 and 300 °C should produce increasing amounts of II. To the best of our knowledge, this experiment has not yet been performed. Also, valuable insight could be obtained from calorimetric studies.

4. Conclusion

The polymorphism of the commodity chemical CaC_2 is a puzzling and long standing problem. The existence – and especially coexistence – of three different crystal modifications at ambient conditions may point to compositional differences between polymorphs or structural peculiarities. In this work tetragonal CaC_2-I was identified as dynamically unstable and its existence attributed to "disorder". Disorder may be structural (crystal structure and microstructure), compositional or dynamical (large anharmonicities). Accordingly, monoclinic CaC_2-II represents the ground state of stoichiometric CaC_2 and monoclinic CaC_2-III a medium temperature phase. With pressure both monoclinic forms transform into CaC_2-I. Above 500 °C CaC_2 occurs as cubic CaC_2-IV for which C_2 dumbbell moieties are orientationally disordered. It is assumed that CaC_2-IV actually constitutes multiple phases.

The characterization of possible various degrees/states of disorder, along with compositional variations of phase IV, e.g. from temperature dependent in situ experiments at synchrotron and neutron facilities, is considered to be key for a conclusive understanding of the formation of I, II, III and their thermodynamic relation. Such investigations are under way. In addition, the presence of structural disorder in I, II, III as well as possibly carbon deficiency for CaC_2-I needs more detailed investigations. Here PDF analysis of total scattering data (both synchrotron X-ray and neutron) would allow probing local structure and help extracting structural features related to disorder. Lastly we note that the peculiar polymorphism of CaC_2 may originate from its enthalpic instability toward decomposition into Ca_2C_3 and Ca, as recently suggested from theory [18]. In this respect, complex transformation processes of CaC_2-IV upon cooling may be interpreted as an onset to phase segregation.

Acknowledgement

This work was supported by the Swedish Research Council (grant no. 2012-2956). In addition we acknowledge NMR equipment grants from the Swedish Research Council and the Knut and Alice Wallenberg Foundation.

Appendix A. Supplementary material

Supplementary data associated with this article can be found in the online version at http://dx.doi.org/10.1016/j.jssc.2016.04.030.

References

[1] M. Weller, T. Overton, J. Rourke, F. Armstrong, Inorganic Chemistry, 6th edition, Oxford University Press, 2014.
[2] C.E. Housecroft, A.G. Sharpe, Inorganic Chemistry, 4th edition, Prentice Hall, 2012.
[3] G.L. Miessler, P.J. Fischer, D.A. Tarr, Inorganic Chemistry, 5th edition, Prentice Hall, 2013.
[4] Commercialization of Calcium Carbide and Acetylene – Landmark – American Chemical Society ⟨http://www.acs.org/content/acs/en/education/whatischemistry/landmarks/calciumcarbideacetylene.html⟩ (accessed 08.12.15).
[5] W. Sun, Econ. Anal. Chin. Petrol. Chem. Ind. 4 (2013) 29–31.
[6] K.S. Rodygin, G. Werner, F.A. Kucherov, V.P. Ananikov, Chem. Asian J. 11 (2016) 965–976.
[7] H.H. Franck, M.A. Bredig, G. Hoffmann, Z. Anorg. Allg. Chem. 232 (1937) 61–74.
[8] H.H. Franck, M.A. Bredig, K.-H. Kou, Z. Anorg. Allg. Chem. 232 (1937) 75–111.
[9] (a) M.A. Bredig, J. Phys. Chem. 46 (1942) 801–819;
(b) M.A. Bredig, Z. Anorg. Allg. Chem. 298 (1959) 255–257;
(c) M.A. Bredig, Z. Anorg. Allg. Chem. 310 (1961) 338–340.
[10] (a) N.-G. Vannerberg, Acta Chem. Scand. 15 (1961) 769–774;
(b) N.-G. Vannerberg, Acta Chem. Scand. 16 (1962) 1212–1220.
[11] O. Reckeweg, A. Baumann, H.A. Mayer, J. Glaser, H.-J. Meyer, Z. Anorg. Allg. Chem. 625 (1999) 1686–1692.
[12] J. Glaser, S. Dill, M. Marzini, H.A. Mayer, H.-J. Meyer, Z. Anorg. Allg. Chem. 627 (2001) 1090–1094.
[13] M. Knapp, U. Ruschewitz, Chem. Eur. J. 7 (2001) 874–880.
[14] A. Kulkarni, K. Doll, J.C. Schön, M. Jansen, J. Phys. Chem. B 114 (2010) 15573–15581.
[15] D. Benson, Y. Li, W. Luo, R. Ahuja, G. Svensson, U. Häussermann, Inorg. Chem. 52 (2013) 6402–6406.
[16] Y.-L. Li, W. Luo, Z. Zeng, H.-Q. Lin, H. Mao, R. Ahuja, Proc. Natl. Acad. Sci. USA 110 (2013) 9289–9294.
[17] J. Nylén, S. Konar, P. Lazor, D. Benson, U. Häussermann, J. Chem. Phys. 137 (2012) 224507.
[18] Y.-L. Li, S.-N. Wang, A.R. Oganov, H. Gou, J.S. Smith, T.A. Strobel, Nat. Commun. 6 (2015) 6974.
[19] J. Rodriguez-Carvajal, Abstracts of the Satellite Meeting on Powder Diffraction of the XV Congress of the IUCr, 1990, p. 127.
[20] H.K. Mao, J. Xu, P.M. Bell, J. Geophys. Res. 91 (1986) 4673–4676.
[21] (a) P.E. Blöchl, Phys. Rev. B 50 (1994) 17953–17979;
(b) G. Kresse, D. Joubert, Phys. Rev. B 59 (1999) 1758.
[22] (a) G. Kresse, J. Hafner, Phys. Rev. B 48 (1993) 13115–13118;
(b) G. Kresse, J. Furthmüller, Comp. Mater. Sci. 6 (1996) 15–50.
[23] J.P. Perdew, K. Burke, M. Ernzerhof, Phys. Rev. Lett. 77 (1996) 3865–3868.
[24] H.J. Monkhorst, J.D. Pack, Phys. Rev. B 13 (1976) 5188–5192.
[25] P.E. Blöchl, O. Jepsen, O.K. Andersen, Phys. Rev. B 49 (1994) 16223–16233.
[26] P. Giannozzi, S. Baroni, N. Bonini, M. Calandra, R. Car, C. Cavazzoni, D. Ceresoli, G.L. Chiarotti, M. Cococcioni, I. Dabo, A.D. Corso, S. de Gironcoli, S. Fabris, G. Fratesi, R. Gebauer, U. Gerstmann, C. Gougoussis, A. Kokalj, M. Lazzeri, L. Martin-Samos, N. Marzari, F. Mauri, R. Mazzarello, S. Paolini, A. Pasquarello, L. Paulatto, C. Sbraccia, S. Scandolo, G. Sclauzero, A.P. Seitsonen, A. Smogunov, P. Umari, R.M. Wentzcovitch, J. Phys. Condens. Matter 21 (2009) 395502.
[27] D. Vanderbilt, Phys. Rev. B 41 (1990) 7892–7895.
[28] (a) M.V. Stackelberg, Naturwissenschaften 18 (1930) 305–306;
(b) M.V. Stackelberg, Z. Phys. Chem. Abt. B 9 (1930) 437.
[29] R. Juza, H.-U. Schuster, Z. Anorg. Allg. Chem. 311 (1961) 62–75.
[30] The transformation of II to III at around 200 °C occurs without noticeable thermal event in DSC measurement [12].
[31] O.O. Kurakevych, T.A. Strobel, D.Y. Kim, G.D. Cody, Angew. Chem. Int. Ed. 52 (2013) 8930–8933.
[32] (a) G. Grimvall, B. Magyari-Köpe, V. Ozoliņš, K.A. Persson, Rev. Mod. Phys. 84 (2012) 945–986;
(b) C. Asker, A.B. Belonoshko, A.S. Mikhaylushkin, I.A. Abrikosov, Phys. Rev. B 77 (2008) 220102;
(c) V. Ozolins, Phys. Rev. Lett. 102 (2009) 065702.
[33] (a) X. Ma, F. Xu, T.M. Atkins, A.M. Goforth, D. Neiner, A. Navrotsky, S. M. Kauzlarich, Dalton Trans. (2009) 10250–10255;
(b) X. Ma, F. Wu, S.M. Kauzlarich, J. Solid State Chem. 181 (2008) 1628–1633;
(c) T. Yi, S. Chen, S. Li, H. Yang, S. Bux, Z. Bian, N.A. Katcho, A. Shakouri, N. Mingo, J.-P. Fleurial, N.D. Browning, S.M. Kauzlarich, J. Mater. Chem. 22 (2012) 24805–24813.
[34] S. Konar, U. Häusserman, G. Svensson, Chem. Mater. 27 (2015) 2566–2575.
[35] (a) V. Vohn, W. Kockelmann, U. Ruschewitz, J. Alloy. Compd. 284 (1999) 132–137;
(b) V. Vohn, M. Knapp, U. Ruschewitz, J. Solid State Chem. 151 (2000) 111–116.
[36] B. Wrackmeyer, K. Horchler, A. Sebald, L.H. Merwin, C. Ross II, Angew. Chem. Int. Ed. 29 (1990) 807–809.
[37] I. Efthimiopoulos, G.V. Vajenine, E. Stavrou, K. Syassen, St. Liebig, U. Ruschewitz, M. Hanfland, Acta Cryst. A66 (2010) s197.